e-Journal of Nondestructive Testing - ISSN 1435-4934 - www.ndt.net

EWSHM 2024
11th European Workshop on Structural Health Monitoring

Reliability Assessment of Damage Localization Techniques for Guided Wave-based Structural Health Monitoring Systems in Composite Stiffened Structures

Ahmed BAYOUMI [1], Enes SAVLI [2], Inka MUELLER [1], Kilian TSCHÖKE [2], Vittorio MEMMOLO [3], Jochen MOLL [4,5]

[1] Bochum University of Applied Sciences, Bochum, Germany, Ahmed.Bayoumi@hs-bochum.de, Inka.Mueller@hs-bochum.de

[2] Fraunhofer Institute for Ceramic Technologies and Systems IKTS, Dresden, Germany, enes.savli@ikts.fraunhofer.de, kilian.tschoeke@ikts.fraunhofer.de

[3] University of Naples "Federico II", Naples, Italy, vittorio.memmolo@unina.it

[4] Goethe University Frankfurt, Frankfurt, Germany

[5] University of Siegen, Siegen, Germany, jochen.moll@uni-siegen.de

Abstract. In Guided Wave-based Structural Health Monitoring (GWSHM) systems, the reliability assessment is of utmost importance. The primary focus is the smallest damage that can be detected with 90 percent probability and 95 percent confidence. However, the probability of correct damage localization is equally crucial as the probability of detection. In this view, defining the smallest damage that can be localized accurately in a statistically meaningful way is quite challenging.

Several localization techniques have been developed in the literature to localize damage resorting to a GW sensor network, like SAFT and RAPID. This article investigates the reliability of such SHM systems with these localization techniques using an experimental data set from the Open Guided Waves (OGW) platform and compares it with predictions obtained via a simulation model using the EFIT method. A carbon fibre-reinforced plate-like structure reinforced by an omega stringer and a GWSHM system employing twelve piezoceramic transducers bonded over the surface to excite and receive guided waves are used. Pseudo damage of thirteen different sizes are attached to three different locations using a damping tacky tape. Moreover, the EFIT modelling tool is used to simulate the experiment with an extensive number of damage scenarios at the defined three damage locations with a high degree of consistency with the experimental data, facilitating a more robust analysis. The outcome concerning the influence and correlation between damage size on localization accuracy, considering various localization techniques, were explored and discussed. Finally, the reliability assessment allowed to establish the performance of the localization approaches in a rigorous way.

Keywords: Structural Health Monitoring systems; Open Guided Waves platform; Localization; Reliability assessment; Probability of localization

https://doi.org/10.58286/29762

1 Introduction

According to the damage tolerance paradigm, maintaining critical structures require continuous inspections over the lifespan to verify the presence of any defect. This procedure is quite critical as well as very demanding, especially for composite structures. However, it can be enhanced through Structural Health Monitoring (SHM) systems using permanently distributed sensors to enable continuous inspection and establish a predictive maintenance. Several approaches are available to predict failures [1]. Among them, wave propagation-based techniques respond to the requirements for an integrated and self-sensed structure. They exploit propagation and reflection of elastic ultrasonic waves in solids as they are affected by any media variation, including damage. Using pitch–catch techniques, damage presence, location and severity can be estimated through different methods [2], [3].

Rytter and Farrar categorize SHM system into four distinct levels presented in order: detection, localization, severity assessment, and prognostics [4], [5]. Localization is the second level, which is engaged once damage has been detected. Within the SHM systems that based on guided wave propagation, there is a wide variety of localization methods available [1], [6], [7]. Among them, localization via probability-based approaches is widely used and has been reported to be effective in detecting damages in complex geometry structures [8], [9]. Probability-based approaches to localization typically employ damage indices, which quantify the integrity of paths within a network of transducers in various forms. This enables the system to infer the likelihood of damage presence and its location within the structure.

However, having a system for SHM replacing current inspection procedures requires the reliability to be assessed properly. While a sound background about damage identification reliability assessment is present in the literature using probability of detection approaches for NDT and the community is about to adopt these concepts with necessary changes to SHM [10], there is not much attempt to quantify damage localization. Bayoumi et, al. [11] presented a quantitative metric to quantify the location accuracy, Probability of Localization (POL). POL analysis is a cumulative distribution function aiming to shade light on the smallest detectable defect within a certain distance tolerance of damage location. The main output of the POL analysis is the damage size $A_{90|95}$, which is the smallest damage that can be localized within a certain tolerance with 90 % probability and 95% confidence. This metric is proposed within this paper to assess the quality of various localization techniques.

Despite the high relevance of a POL for applications, it requires extensive experimental campaigns to get to a statistically meaningful dataset. However, numerical simulation can aid the analysis supporting performance assessment [12]. Within this context, this paper applies the POL approach to two different localization techniques based on probability diagnostic imaging comparing the performance thereof in correctly estimating damage position in composite structures. In addition, the dataset is extended via numerical simulation to explore model assisted approaches. The following section starts by describing the experimental and simulation datasets. It then follows the two localization techniques and ends with the main procedures required for the estimation of POL curves and their confidence interval. Then, the results and discussion section are presented, highlighting the main comparison of these two localization techniques using the POL approach on the experimental data as well as the simulation one. Finally, a summary is presented.

1. Description of Data Set and Description of Concepts

1.1 Experimental dataset (OGW platform)

The experimental dataset for testing the concepts can be accessed via the OGW online platform [13]. The dataset utilizes a 500 mm × 500 mm carbon fibre-reinforced polymer stiffened by a central omega stringer and equipped with twelve piezoceramic transducers, (see Figure 1). The excited signal is a Hann-windowed sinusoidal signal with a central frequency of 40 kHz and five cycles. More detailed information regarding the experimental layout can be found in [14]. Reversible damage is simulated with elliptical metallic plates of 13 different sizes (ranging from 49.48 mm² to 2090.53 mm²), attached by vacuum sealant tape at three defined positions (D1, D2, and D3). Consequently, the dataset consists of 66 actuator-receiver paths, with three distinct damage positions, D1, D2, and D3, for each of the 13 damage sizes. However, this paper mainly focuses on 36 paths that cross the omega stringer.

1.2 Simulation dataset

The experimental setup is simulated at the selected frequency using EFIT numerical model to compare localisation results and evaluate the model assistance in assessing the probability of localization. EFIT is a numerical scheme for investigating all types of elastic wave propagation and is becoming a suitable tool for the design of GW-based SHM systems. [15]. Briefly, it advances with integral form of the velocity–stress formulation on a staggered spatial and temporal grid similar to the velocity–stress finite difference method (VS-FDM). For further information, the reader is recommended to refer [16].

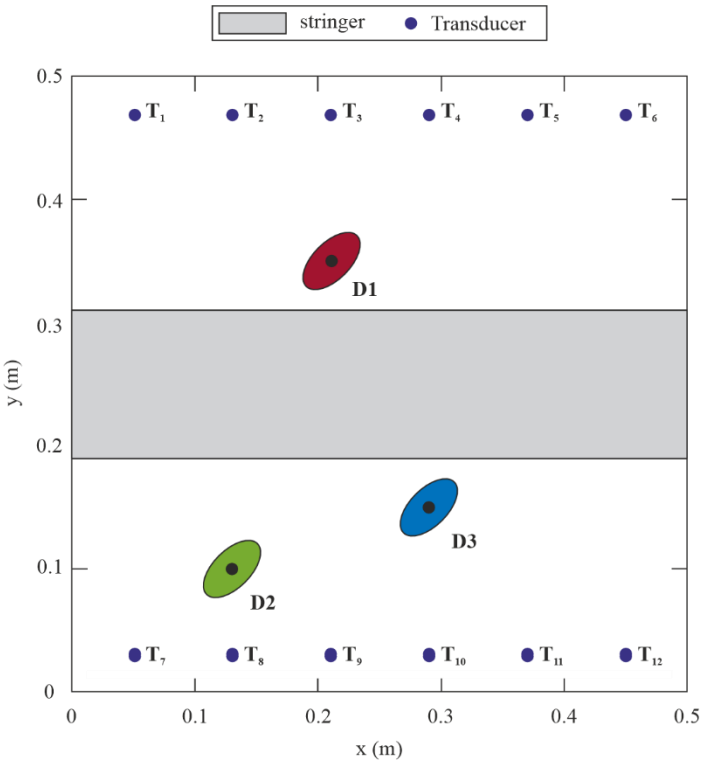

Figure 1: Schematic illustration of the experimental design; the location of transducers and the three different positions of the damage [14].

For the simulations, the stringer and the plate were modelled with homogenised material properties corresponding to the original stiffness of the composite laminate with reference to the Equivalent Single Layer (ESL) method. The entire structure discretized using the grid step size as dx=dy=1 mm for the plane directions and dz=0.5 mm for the thickness direction, which falls within the 20–40 nodes per wavelength range, thus resulting in nearly 2 million cells to be computed. EFIT simulations use a smaller time step by definition [17], so a time step of Δt=3.4×10-8 s was chosen for the 600 μs simulation period. The total computation time for each transient solution was slightly about 2 h and required just 8 GB RAM in a medium level workstation. A total of 48 simulations were performed and data collected from transducer points (1 baseline + three different damage scenarios) to evaluate the SHM system and to assess the localisation performance.

1.3 Localization techniques

1.3.1 Probability diagnostic imaging using signal correlation

This localization technique is used to determine the localization of the damage [18] by calculating the intensity factor ($I(x,y)$) for each location on the plate based on the correlation coefficient-based damage indicator, $\mathrm{DI}_{CC,k}$,values, expressed as:

$$\mathrm{DI}_{CC,k} = \left| 1 - \frac{\sum_{i=1}^{N} S_{H,k,i}\, S_{D,k,i} - \sum_{i=1}^{N} S_{H,k,i} \sum_{i=1}^{N} S_{D,k,i}}{\sqrt{\sum_{i=1}^{N} S_{H,k,i}^2 - \left(\sum_{i=1}^{N} S_{H,k,i}^2\right)^2} \cdot \sqrt{\sum_{i=1}^{N} S_{D,k,i}^2 - \left(\sum_{i=1}^{N} S_{D,k,i}^2\right)^2}} \right|,$$

where $k = 1,2,..,N_p$ is the maximum number of paths, S is the recorded measurement, H refers to the recorded measurement at the pristine state, and D for the damaged one. N is the sampling points of the acquired signal. Then, the $I(x,y)$ can be expressed as:

$$I(x,y) = \sum_{k=1}^{N_p} \left(DI_{CC,k}\right) \left(\frac{-1}{\tau - 1} \cdot R(x,y) + \frac{\tau}{\tau - 1}\right),$$

$$k = 1,2,\ldots,N_p;\ i,j = 1,2,\ldots,N,\ but\ i \neq j,$$

where $\tau = 1.05$ is scaling factors controlling the area influenced by the transducer pairs (i.e., from the i_{th} actuator located at (x_i,y_i) to the j_{th} sensor located at (x_i,y_i)) and $R(x,y)$ is a location-specific factor which forms an elliptical shape around the actuator and sensor of a specific path. This way, each path has an influence on the intensity factor for each pixel (x,y). The higher the $\mathrm{DI}_{CC,k}$ value for an actuator-sensor pair, the higher the probability of damage at the pixels near the k_{th} path. Finally, the location of the damage is estimated as the center of the area of the highest 5% of $I(x,y)$ values, as shown in Figure 2(a).

1.3.2 Meshless diagnostic imaging using signal energy

The second localization algorithm relies on a meshless approach which defines the damage location probability from the intersection nodes of actuator-receiver paths most affected by the damage [19]. To select those paths, an energy-based indicator is used, comparing the energy of each single actuator receiver path in the pristine state of the structure with the current condition. For each actuator receiver pair, the generalized energy is obtained as:

$$E_Q = \sum_{i=1}^{N} S_{Q,k,i}^2,$$

where Q refers to the state of the structure, H for the pristine state and D for the damaged state. Then, the damage indicator, accounting for the nominal energy difference between pristine and current structure state, can be calculated as follow:

$$DI(E) = \frac{|E_D - E_H|}{E_H},$$

To reconstruct damage, the (sensitive) paths are selected when exhibiting a damage indicator higher than the threshold defined by noise level in unsupervised mode. From the intersection of sensitive paths, few emerging points create a mesh where structural condition is parameterized according to the average value of the damage indicator exhibited by the intersecting lines of sight. The coordinates of such resulting nodes, whose weight is the resulting indicator, are passed to an algorithm which estimates the damage location fitting a surface on the scattered data and reporting a tomographic representation of damaged area. Finally, the location of the damage is estimated as the centre of the 95% isoline, as shown in Figure 2(b).

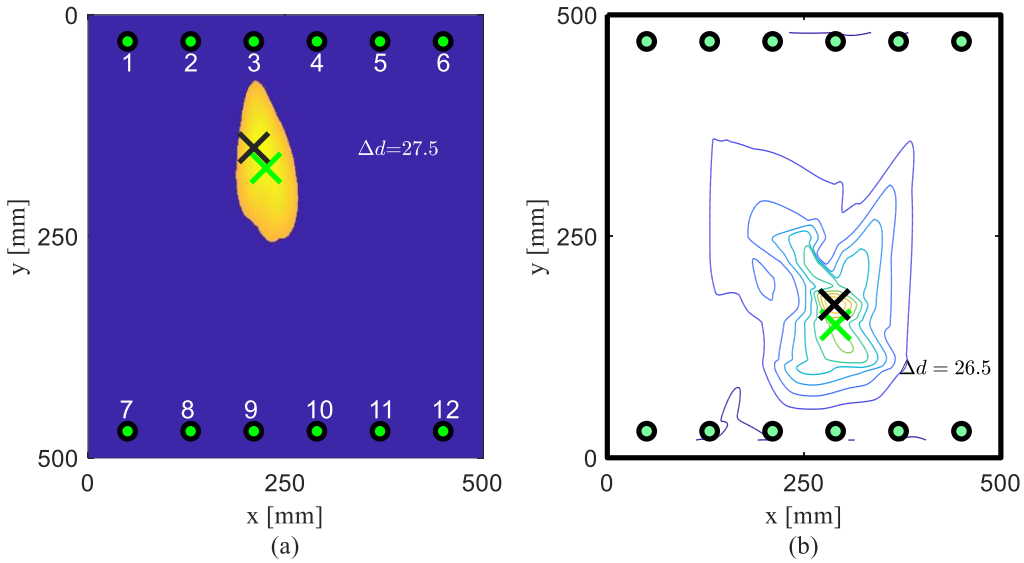

Figure 2: Resultant output of the localization techniques (a) probability diagnostic imaging using signal correlation at damage position D1 (b) meshless diagnostic imaging using signal energy at damage position D3.

1.4 Probability of Localization (POL)

The POL is calculated based on the method of the classical Probability of Detection (POD) approach using signal response $\hat{a}$, versus damage size A method, as described in MILHDBK1823 [20]. The main difference is using Δd distance instead of signal response $\hat{a}$.

The POL procedure starts from the application of linear regression analysis and setting the threshold, also known as tolerance, to calculate the POL parameters. Then, using the maximum likelihood estimator and the Delta method to estimate the covariance matrix of linear regression parameters and then transform it to the covariance matrix of POL parameters, μ_{POL} and σ_{POL}, using a transformation matrix. Finally, it uses the covariance matrix of POL parameters to calculate the 95% Wald confidence interval.

The POL curve, is a cumulative distribution function, can be expressed as:

$$POL = 1 - \Phi\left[\frac{damage\ size\ A - \mu_{POL}}{|\sigma_{POL}|}\right],$$

where Φ is the cummulative distribution function. Finally, the $A_{90|95}$ can be expressed as:

$$A_{90|95} = \mu_{POL=90\%} + z(\alpha) \cdot \sigma_{POL=90\%},$$

where z(α) is 1.645 and represents the 95% confidence bound value. Damage size $A_{90|95}$ is the smallest damage size that can be detected with probability 90% and 95% Wald confidence interval within a certain Δd distance.

The dataset used for the analysis can be either experimental or simulation-based. Regardless the dataset used, either simulation or experimental, the POL analysis will be applied. The procedures for application of the simulation-based POL analysis are the same as for the experimental-based POL analysis.

2 Results

The main point of comparison considered is the output of the POL approach. The threshold is set at 7 cm for estimating the POL curves and their confidence interval. The generated POL using the probability diagnostic imaging technique using signal correlation is first presented. Then, the generated POL curves using the second localization technique follows.

Figure 3 shows the relationship between Δd the damage size A for the experimental and simulation damage scenario data sets. The results indicate a good agreement between the two data sets, which suggests the accuracy of the EFIT numerical model in generating a simulation-based POL. The slope of the dataset decreases until damage size number 5, after which the trend seems to reach its saturation. This trend is consistent for both datasets, the experimental and simulation one.

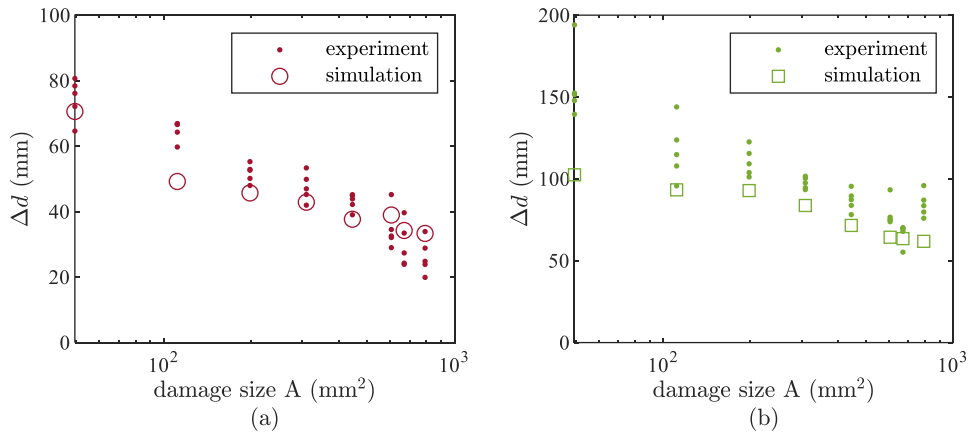

Figure 3: relation between Δd and damage size A (a) probability diagnostic imaging using signal correlation at D1 damage position (b) using meshless diagnostic imaging using signal energy at D2 damage position.

Figures 4(a) and 4(b) present the experimental-based POL and simulation-based POL curves of the probability diagnostic imaging using signal correlation. While Figures 5(a) and 5(b) show the results of the meshless diagnostic imaging using signal energy. The experimental-based POL and simulation-based POL analyses were performed for all three different damage positions, D1, D2 and D3.

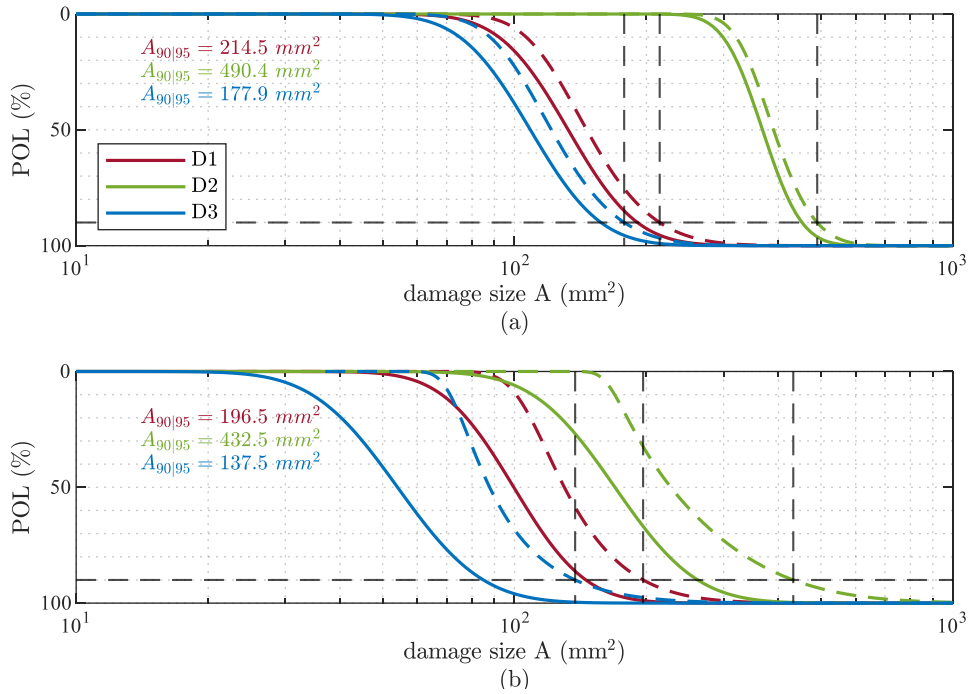

Figure 4: POL analysis using probability diagnostic imaging (a) experimental-based POL analysis (b) simulation-based POL analysis for reversible defects at three different positions.

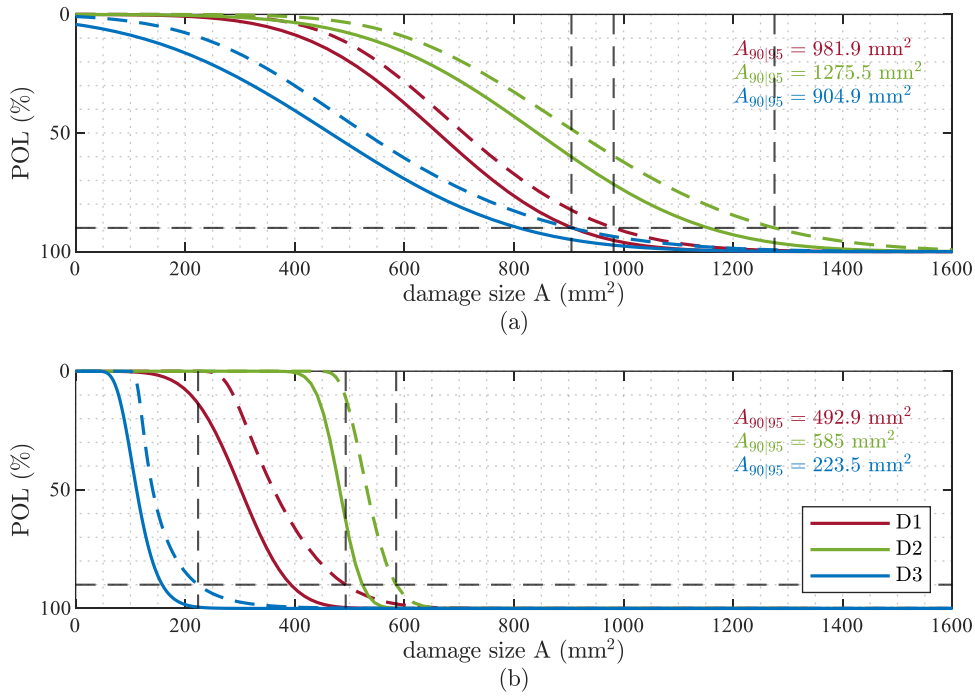

Figure 5: POL analysis using meshless diagnostic imaging (a) experimental-based POL analysis (b) simulation-based POL analysis for reversible defects at three different positions.

The results of the simulation-based POL analysis show lower values for the main output, $A_{90|95}$, compared to the experimental-based POL analysis. Additionally, it can be noticed that the smallest $A_{90|95}$value either using the probability diagnostic imaging or meshless diagnostic imaging for three damage positions are in the same sequence as D3, followed by D1 and D2 positions for both the experimental-based POL and simulation-based POL analysis.

3 Discussion

The results show the added value of applying the POL approach on the example of two localization techniques using experimental and simulation-based data. The localization techniques are probability and meshless diagnostic imaging using signal correlation and energy.

Figures 3(a) and (b) show the relationship between Δd distance and damage size A using probability and meshless diagnostic imaging. There is a good agreement between the simulation and experimental data, which reflects the EFIT effectiveness in modelling wave-damage interactions.

Figures 4(a) and 5(a) show the POL analysis of both localization techniques using the experimental dataset. The smallest detectable damage with 90% probability and 95% confidence interval is much higher when performing meshless diagnostic imaging using signal energy than performing probability diagnostic imaging using signal correlation. When performing signal energy, the influence of noise is much higher on signal energy than signal correlation. Moreover, a major reason for the higher $A_{90|95}$ is that the meshless method was developed for SHM systems, in which the sensors are distributed around the structure at all edges in the first place. In contrast, only two rows of sensors are a "worst case" scenario for the described meshless diagnostic. Further investigation is required to explore different damage indicators for meshless diagnostic imaging localization techniques and determine whether they will yield a better result.

Figures 4(b) and 5(b) indicate the POL analysis of the two localization techniques based on simulation data. The $A_{90|95}$values in the simulation dataset are, especially for the meshless method, considerably lower compared to the experimental dataset. This is because the simulation models do not account for system uncertainties. The primary variability in the dataset is caused by the linear regression model, which defines its parameters. Further investigation is necessary to assess the feasibility of incorporating system uncertainty in the simulation dataset and its impact on the simulation-based POL analysis for specific localization techniques.

The $A_{90|95}$values of experimental-based POL and simulation-based POL analysis at damage position D1 and D3 are significantly lower than those obtained at damage position D2. This is because the positions D1 and D3 are situated closer to the vertical central line of the transducer network and away from the distributed sensors, while this is not the case for D2 damage position. Such result demonstrates how damage localization reliability strongly depends upon damage position within the transducer network just like detection algorithm.

4 Conclusion

Within this article, it has been shown that it is necessary to use concepts like probability of localization approach in order to investigate the performance of localization techniques. While for both exemplary techniques, it is possible to show prove of concept results, the POL analysis reveals important additional information. On the one hand, the difference between experimental-based POL and simulation-based POL differs significantly for the two localization techniques, while the localization results in the first place give the impression of similar level of agreement between simulation and experiment. Moreover, the performance of the localization techniques is highly damage location specific.

The choice of the localization technique is a vital factor in assessing the reliability of GWSHM systems. According to the results, the probability diagnostic imaging using signal correlation has a higher localization accuracy than meshless diagnostic imaging using signal energy using this sensor network setup. Nevertheless, the results are highly setup dependent

of the transducer network. It is, therefore, absolutely necessary, to investigate the performance for each use case separately. In conclusion, POL approach helps analysing the performance accuracy. It is visible that, depending on the chosen damage localization algorithm, the output information of the POL approach may differ significantly.

The collaboration of the authors was supported by the DFG within the Scientific Network Towards a holistic quality assessment for guided wave-based SHM (project number 424954879)

5 References

[1] Z. Su and L. Ye, *Identification of damage using Lamb waves: from fundamentals to applications*, vol. 48. Springer Science & Business Media, 2009.
[2] V. Giurgiutiu, *Structural health monitoring: with piezoelectric wafer active sensors*. Elsevier, 2007.
[3] J. L. Rose, *Ultrasonic Guided Waves in Solid Media*. Cambridge: Cambridge University Press, 2014. doi: 10.1017/CBO9781107273610.
[4] A. Rytter, 'Vibrational Based Inspection of Civil Engineering Structures', 1993.
[5] C. R. Farrar and K. Worden, 'An introduction to structural health monitoring', *Philos. Trans. R. Soc. Math. Phys. Eng. Sci.*, vol. 365, no. 1851, pp. 303–315, Dec. 2006, doi: 10.1098/rsta.2006.1928.
[6] L. Schubert, R. Schwerz, M. Leibowitz, U. Lieske, and B. Frankenstein, 'Guided wave based SHM approach using SAFT-algorithm for impact detection in composite materials', 2011, Accessed: Apr. 12, 2024. [Online]. Available: https://publica.fraunhofer.de/entities/publication/e124362d-bced-40be-8083-852d25220037
[7] R. Neubeck, C. Kexel, and J. Moll, 'Matrix techniques for Lamb-wave damage imaging in metal plates', *Smart Mater. Struct.*, vol. 29, no. 11, p. 117003, 2020.
[8] M. Moix-Bonet, B. Eckstein, and P. Wierach, 'Probability-based damage assessment on a composite door surrounding structure', *Proc. 8th EWSHM*, 2016, Accessed: Apr. 12, 2024. [Online]. Available: https://www.ndt.net/events/EWSHM2016/app/content/Paper/135_MoixBonet_Rev1.pdf
[9] M. M. Malatesta, R. Neubeck, J. Moll, K. Tschöke, and L. De Marchi, 'Double-stage DMAS with fresnel zone filtering in guided waves damage imaging', *IEEE Trans. Ultrason. Ferroelectr. Freq. Control*, vol. 69, no. 5, pp. 1751–1762, 2022.
[10] I. Mueller *et al.*, 'Performance Assessment for Artificial Intelligence-Based Data Analysis in Ultrasonic Guided Wave-Based Inspection: A Comparison to Classic Path-Based Probability of Detection', in *European Workshop on Structural Health Monitoring*, P. Rizzo and A. Milazzo, Eds., in Lecture Notes in Civil Engineering. Springer International Publishing, 2023.
[11] A. Bayoumi, T. Minten, and I. Mueller, 'Determination of Detection Probability and Localization Accuracy for a Guided Wave-Based Structural Health Monitoring System on a Composite Structure', *Appl. Mech.*, vol. 2, no. 4, pp. 996–1008, Dec. 2021, doi: 10.3390/applmech2040058.
[12] K. Tschoke *et al.*, 'Feasibility of Model-Assisted Probability of Detection Principles for Structural Health Monitoring Systems Based on Guided Waves for Fiber-Reinforced Composites', *IEEE Trans. Ultrason. Ferroelectr. Freq. Control*, vol. 68, no. 10, pp. 3156–3173, Oct. 2021, doi: 10.1109/tuffc.2021.3084898.
[13] J. Moll *et al.*, 'Open Guided Waves: online platform for ultrasonic guided wave measurements', *Struct. Health Monit.*, vol. 18, no. 5–6, pp. 1903–1914, Dec. 2018, doi: 10.1177/1475921718817169.
[14] J. Moll *et al.*, 'Guided waves for damage detection in complex composite structures: the influence of omega stringer and different reference damage size', *Appl. Sci.*, vol. 10, no. 9, p. 3068, 2020.
[15] E. Savli, J. Lefèvre, C. Willberg, and K. Tschöke, 'Numerical Simulations in Ultrasonic Guided Wave Analysis for the Design of SHM Systems—Benchmark Study Based on the Open Guided Waves Online Platform Dataset', *Aerospace*, vol. 10, no. 5, p. 430, 2023.
[16] F. Schubert, 'Numerical time-domain modeling of linear and nonlinear ultrasonic wave propagation using finite integration techniques—-theory and applications', *Ultrasonics*, vol. 42, no. 1–9, pp. 221–229, 2004.
[17] K. Tschöke and H. Gravenkamp, 'On the numerical convergence and performance of different spatial discretization techniques for transient elastodynamic wave propagation problems', *Wave Motion*, vol. 82, pp. 62–85, 2018.
[18] Z. Su and L. Ye, *Identification of damage using Lamb waves: from fundamentals to applications*, vol. 48. Springer Science & Business Media, 2009.
[19] V. Memmolo, N. D. Boffa, L. Maio, E. Monaco, and F. Ricci, 'Damage localization in composite structures using a guided waves based multi-parameter approach', *Aerospace*, vol. 5, no. 4, p. 111, 2018.
[20] C. Annis, E. Bray, H. Hardy, and P. Hoppe, 'Nondestructive evaluation system reliability assessment', *U. S. Dep. Def. Wright-Patterson AFB Handb. MIL-HDBK-1823A*, 2009.